Article

Substrate Deformation Predicts Neuronal Growth Cone Advance

Ahmad I. M. Athamneh,[1,2] Alexander X. Cartagena-Rivera,[2,3] Arvind Raman,[2,3] and Daniel M. Suter[1,2,4,*]
[1]Department of Biological Sciences, [2]Birck Nanotechnology Center, [3]School of Mechanical Engineering, and [4]Bindley Bioscience Center, Purdue University, West Lafayette, Indiana

ABSTRACT Although pulling forces have been observed in axonal growth for several decades, their underlying mechanisms, absolute magnitudes, and exact roles are not well understood. In this study, using two different experimental approaches, we quantified retrograde traction force in *Aplysia californica* neuronal growth cones as they develop over time in response to a new adhesion substrate. In the first approach, we developed a novel method, to our knowledge, for measuring traction forces using an atomic force microscope (AFM) with a cantilever that was modified with an *Aplysia* cell adhesion molecule (apCAM)-coated microbead. In the second approach, we used force-calibrated glass microneedles coated with apCAM ligands to guide growth cone advance. The traction force exerted by the growth cone was measured by monitoring the microneedle deflection using an optical microscope. Both approaches showed that *Aplysia* growth cones can develop traction forces in the 10^0–10^2 nN range during adhesion-mediated advance. Moreover, our results suggest that the level of traction force is directly correlated to the stiffness of the microneedle, which is consistent with a reinforcement mechanism previously observed in other cell types. Interestingly, the absolute level of traction force did not correlate with growth cone advance toward the adhesion site, but the amount of microneedle deflection did. In cases of adhesion-mediated growth cone advance, the mean needle deflection was 1.05 $\pm$ 0.07 μm. By contrast, the mean deflection was significantly lower (0.48 $\pm$ 0.06 μm) when the growth cones did not advance. Our data support a hypothesis that adhesion complexes, which can undergo micron-scale elastic deformation, regulate the coupling between the retrogradely flowing actin cytoskeleton and apCAM substrates, stimulating growth cone advance if sufficiently abundant.

INTRODUCTION

Mechanical forces play a fundamental role during development and regeneration of the nervous system (1,2). Studies have shown that neurites are under permanent tension and that their growing tip, the neuronal growth cone, can develop traction forces (3–6). In addition, in vitro and in vivo application of tensile forces on neurites promotes their elongation (7–10). Furthermore, mechanical force plays a fundamental role in the ability of neuronal growth cones to sense and respond to the stiffness of the extracellular environment (11). In advancing growth cones, traction force is generated as a result of coupling of the myosin-powered retrograde F-actin flow to a stationary extracellular substrate (12–16). Coupling is mediated by adhesion receptors, such as immunoglobulin superfamily cell adhesion molecules and N-cadherin that connect to the actin cytoskeleton via linkage proteins (13,16,17). The vector sum of traction forces resulting from substrate-cytoskeletal coupling throughout the whole area of the growth cone opposes the tension that is acting along the neurite (18–20). Growth cone sensing and response to mechanical cues is thought to be mediated through 1) the slowing of F-actin flow as a result of coupling to the extracellular substrate (11,13,21,22) and 2) mechanosensitive ion channels (23–26). Despite these advances in the field of neuronal mechanics, the precise mechanism of force generation and transmission in the growth cone as well as the role of force in axonal guidance and growth are not fully understood. Specifically, the development of traction forces as growth cones encounter new adhesion substrates has not been quantified with high-temporal and spatial resolution to date. Such quantification is necessary to establish correlations between force and other known quantifiable molecular and biophysical parameters within the cell, which will lead to a better understanding of the fundamental role of forces in axonal growth and guidance.

Different experimental methodologies have been utilized to quantify forces in axons and growth cones including the use of 1) force-calibrated microneedles (3,4,9,27–29), 2) traction force microscopy on flexible substrates (11,14,18–20,23,30) or fabricated nanowire arrays (31), 3) optical tweezers (16,32–34), 4) atomic force microscope (AFM) (35), and 5) microfabricated silicon-based micromechanical force sensors (6,36). Force-calibrated microneedles were employed in the earliest quantitative work and provided a global view of mechanical force at the whole neuron and neurite level, but the details of force generation and distribution at the growth cone level remained unclear (4,5,8,27–29,37,38). Traction force microscopy enabled quantitative force measurements at the growth cone level and presented high-resolution

Submitted March 27, 2015, and accepted for publication August 12, 2015.
*Correspondence: dsuter@purdue.edu
Editor: Jochen Guck

0006-3495/15/10/1358/14
http://dx.doi.org/10.1016/j.bpj.2015.08.013

visualization of force distribution in the growth cone (18–20,23). However, the uniform substrates used in these experiments provide the growth cone with the same mechanical and molecular stimuli from all directions simultaneously. The substrate uniformity issue can be circumvented using optical tweezers trapping a bead coated with an adhesion protein for the growth cone to interact with. However, optical tweezers typically cannot provide enough force to trigger growth cone advance (16,32–34), although in the case of spinal commissural neurons, 0.063 nN was sufficient to redirect axons toward immobilized netrin-1 beads (39).

Our previous research has shown that growth cone advance can be induced by mechanically restraining an *Aplysia* cell adhesion molecule (apCAM)-coated bead coupled to the actomyosin network in the growth cone peripheral (P) domain (13). This restrained bead interaction (RBI) assay allowed analysis of cytoskeletal dynamics and signaling underlying adhesion-mediated growth cone advance (40–43). Studies using the RBI assay provided strong evidence for the role of force in regulating growth cone motility and guidance; however, growth cone traction forces have not been quantified using this assay. To that end, we have used two different experimental approaches to quantify retrograde traction forces in the growth cones of *Aplysia californica* bag cell neurons as they develop over time in response to a new adhesion substrate. In the first approach, we developed a new method, to our knowledge, for measuring traction forces using an AFM with an apCAM-coated colloidal cantilever. In the second approach, we used force-calibrated glass microneedles coated with apCAM ligands to guide the advance of *Aplysia* growth cones. Both microneedle and AFM approaches showed that *Aplysia* growth cones are capable of developing traction forces on the order of 10^0 to 10^2 nN, which is an order of magnitude higher than previously reported for other experimental methods and/or neuronal cell types. Moreover, our results show that traction force is directly correlated to the stiffness of the microneedle. Contrary to our initial expectations, our results revealed that the level of force produced during an adhesive contact does not correlate with growth cone advance behavior, but the level of microneedle deflection does. In cases where the growth cone advanced in the direction of the adhesion site, the mean microneedle deflection was 1.05 ± 0.07 μm. By contrast, the mean deflection was significantly lower (0.48 ± 0.06 μm) when the growth cones did not advance in response to the adhesion substrate (i.e., microneedle). Our results provide novel insights, to our knowledge, into the significance of the level of substrate deformation as opposed to the level of traction force for the regulation of adhesion-mediated directional growth cone advance. We argue that the level of substrate deformation likely originates from the size of the underlying elastic cytoskeletal structures involved in clutch formation.

MATERIALS AND METHODS

Aplysia californica neuronal cell culture

Aplysia bag cell neurons were dissected and cultured in L15 medium (Invitrogen, Carlsbad, CA) supplemented with artificial seawater (400 mM NaCl; 9 mM $CaCl_2$; 27 mM $MgSO_4$; 28 mM $MgCl_2$; 4 mM L-glutamine; 50 μg/ml gentamicin; 5 mM HEPES, pH 7.9) on a glass-bottom dish (Fluorodish Cell Culture Dish, World Precision Instruments, Sarasota, FL) coated with 20 μg/ml poly-L-lysine as previously described (13,44). Cells were kept at 14°C until the time of experiment; typically 1 d after plating.

Measuring retrograde traction force in growth cones using AFM

Karhu et al. (45) showed that frictional-force measurement using AFM was possible in longitudinal imaging mode and provided several advantages over lateral imaging mode. We built on their approach, which is essentially measurement of force parallel to the imaging surface, and we developed a new approach, to our knowledge, for measuring growth cone traction force by monitoring the vertical height of the AFM cantilever as it interacts with the growth cone. Fig. 1 shows an AFM cantilever with attached bead interacting with the P domain of a growth cone. The shape of the cantilever is described by the Euler–Bernoulli equation as follows (46):

$$EI\frac{d^2y}{dx^2} = M(x), \tag{1}$$

where E is the elastic Young's modulus of the cantilever, I is its area moment, d^2y/dx^2 is the local curvature, and $M(x)$ is internal bending moment. The spherical bead of radius R is attached at a distance L from the cantilever base. Note that the end point of the cantilever is to the right of the contact point between the bead and the growth cone surface at the

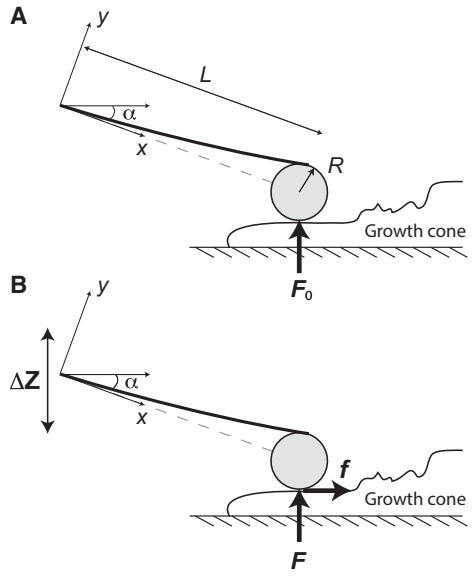

FIGURE 1 Schematic of AFM-based force measurement approach. Illustration depicts the side view of an AFM cantilever modified with apCAM-coated bead interacting with the P domain of a neuronal growth cone (*A*) before and (*B*) after active coupling between the bead and the growth cone cytoskeleton. Before coupling, the net external forces, F_0, acting on the cantilever via the bead are the normal and adhesion forces. After coupling, the net external force F acting on the cantilever via the bead changes because of the introduction of the retrograde traction force f.

bottom of the bead. Thus, the distance from the base of the cantilever to the contact point is $L + R\sin\alpha$, and its position along the y axis is $R(1+\cos\alpha)$. The cantilever shape is then governed by the following:

$$EIy'' = (F\cos\alpha + f\sin\alpha)(L + R\sin\alpha - x) - (F\sin\alpha - f\cos\alpha)(1+\cos\alpha)R, \quad (2)$$

where f is the force exerted by the coupled growth cone cytoskeleton on the cantilever in the direction indicated in Fig. 1, and F is the reaction force (normal and adhesion) in the normal direction. Forces indicated in Fig. 1 are in reality resultant forces representing the sum of forces resulting from the interaction along the total contact area. These forces can be considered point forces because the contact area is very small relative to the size of the bead.

Integrating, we can solve for the slope y′ at any point along the x axis as follows:

$$y'(x) = \frac{1}{EI}\int [(F\cos\alpha + f\sin\alpha)(L + R\sin\alpha - x) - (F\sin\alpha - f\cos\alpha)(1+\cos\alpha)R]dx. \quad (3)$$

Using the boundary condition $y'(0) = 0$, we obtain the following:

$$y'(x) = \frac{1}{EI}\left[(F\cos\alpha + f\sin\alpha)\left(Lx + xR\sin\alpha - \frac{x^2}{2}\right) - (F\sin\alpha - f\cos\alpha)(1+\cos\alpha)Rx\right]. \quad (4)$$

Integrating one more time, we obtain the following cantilever shape:

$$y(x) = \int \frac{1}{EI}\left[(F\cos\alpha + f\sin\alpha)\left(Lx + xR\sin\alpha - \frac{x^2}{2}\right) - (F\sin\alpha - f\cos\alpha)(1+\cos\alpha)Rx\right]dx. \quad (5)$$

Using the boundary condition $y(0) = 0$, we obtain the following:

$$y(x) = \frac{1}{2EI}\left[(F\cos\alpha + f\sin\alpha)\left(Lx^2 + x^2R\sin\alpha - \frac{x^3}{2}\right) - (F\sin\alpha - f\cos\alpha)(1+\cos\alpha)Rx^2\right]. \quad (6)$$

From Eq. 4, the end slope is the following:

$$y'(L) = \frac{L^2}{EI}\left[(F\cos\alpha + f\sin\alpha)\left(\frac{1}{2} + s\sin\alpha\right) - (F\sin\alpha - f\cos\alpha)(1+\cos\alpha)s\right], \quad (7)$$

and from Eq. 6, the end deflection is the following:

$$y(L) = \frac{L^3}{2EI}\left[(F\cos\alpha + f\sin\alpha)\left(\frac{2}{3} + s\sin\alpha\right) - (F\sin\alpha - f\cos\alpha)(1+\cos\alpha)s\right], \quad (8)$$

where $s = R/L$.

The end slope of the cantilever is kept constant by the AFM feedback loop during measurements by adjusting the vertical height of the cantilever as follows:

$$y'(L)_f = y'(L)_0, \quad (9)$$

where $y'(L)_o$ and $y'(L)_f$ are the end slope of the cantilever before and after coupling, respectively.

$$(F\cos\alpha + f\sin\alpha)\left(\frac{1}{2} + s\sin\alpha\right) - (F\sin\alpha - f\cos\alpha) \times (1+\cos\alpha)s = F_0\cos\alpha\left(\frac{1}{2} + s\sin\alpha\right) - F_0\sin\alpha(1+\cos\alpha)s. \quad (10)$$

After some rearrangement, we obtain the following:

$$F = F_0 - f\frac{2s(1+\cos\alpha) + \sin\alpha}{\cos\alpha - 2s\sin\alpha}. \quad (11)$$

By substituting F into Eq. 8, the deflection at end of the cantilever can be expressed in terms of F_0 and f as follows:

$$y(L) = \frac{1}{k}\left[F_0\left(\cos\alpha - \frac{3s}{2}\sin\alpha\right) - \frac{s}{2}\frac{1+\cos\alpha}{\cos\alpha - 2s\sin\alpha}f\right]. \quad (12)$$

Assuming no change to the shape of the growth cone (at least on a short timescale), any change to the vertical height of the cantilever is caused by the introduction of f. Thus, difference in the vertical height z before and after coupling between the bead and the growth cone cytoskeleton retrograde flow is as follows:

$$\Delta z = z_0 - z_f = y_0\cos\alpha - y_f\cos\alpha.$$

This leads to the following:

$$\Delta z = \frac{s}{2k}\frac{1+\cos\alpha}{1 - 2s\tan\alpha}f. \quad (13)$$

Equation 13 shows that the retrograde force f exerted by the growth cone on the bead can be determined by monitoring the change in Z position. Finally, the retrograde force can be calculated using the following simple formula:

$$f = \Delta z\left[\frac{2k}{s}\frac{1 - 2s\tan\alpha}{1+\cos\alpha}\right]. \quad (14)$$

Tipless AFM cantilevers HQ:CSC38/TIPLESS/CR-AU (Mikromasch, Lady's Island, SC) with a nominal spring constant of 0.03 N/m were modified with a 5 μm Ni-NTA silica bead (Micromod, Rostock, Germany) by Novascan Technologies (Ames, IA). Cantilevers were incubated in 0.5 M NaOH for 30 min, washed three times in phosphate-buffered saline (PBS) and incubated in 300 μg/ml recombinant 6His-tagged apCAM purified from baculovirus-infected Sf9 cells (41) in PBS overnight at 4°C. AFM measurements were performed using a commercial MFP-3D-BioAFM system (Asylum Research, Santa Barbara, CA) mounted on an Olympus IX71 (Center Valley, PA) inverted optical microscope, which allows for simultaneous collection of AFM data and phase contrast time-lapse images. The spring constant of the cantilevers was experimentally determined before each experiment using the thermal noise method in culture media (47). Growth cones with the desired orientation were located, and the cantilever

engaged directly onto the growth cone P domain at 0.1 V set point. Real-time *Z* sensor data, which represent the height of the cantilever above the sample, was collected at 1 Hz frequency using the logger function in the MFP-3D software. *Z* sensor data were corrected for drift by subtracting a drift baseline measured by engaging the cantilever on the glass next to the growth cone for at least 10 min. Phase contrast time-lapse images were acquired in 10 s intervals starting immediately after engaging the AFM cantilever.

Preparing microneedles for force measurements

Microneedles for force measurements were prepared by pulling 5 μl glass capillaries (Drummond Scientific Co., Broomall, PA) using a Narishige PP-832 vertical micropipette puller (Narishige, East Meadow, NY). Settings on the puller were adjusted to fabricate microneedles with a closed (beam-like) tapered tip that is ~5 mm long. After pulling, the fine microneedle tip was slightly melted by bringing the tip close to the heating element on the puller to ensure a smooth round tip.

Calibrating microneedles using AFM

We used the MFP-3D-BioAFM system in contact mode and BL-TR-400PB (Olympus) cantilevers to measure the stiffness of microneedles in air (Fig. S1in the Supporting Material). The spring constant of the cantilevers was experimentally determined using the thermal noise method in air (47). The microneedle was mounted on the microscope stage so that its long axis was parallel to the long axis of the AFM cantilevers. A tapping mode image of the microneedle tip was first collected for determination of an exact position of the cantilever with respect to the microneedle tip. Next, force curves were collected on the center of the free end of the microneedle using 50 nN as a trigger point. The collected force data was plotted against the height of the cantilevers minus its deflection as illustrated in Fig. S1. The slope of the linear region represented the microneedle stiffness.

Calibrating microneedles using a laser Doppler vibrometer

Measurements of microneedle stiffness using a laser Doppler vibrometer (LDV) was performed according to Lozano et al. (48). Initially, stiffness measurements were performed using both AFM and LDV for confirmation of accuracy. Later measurements were conducted using LDV only, because results were virtually identical. We used a Polytec MSA-400 scanning LDV (Polytec Gmbh, Waldbronn, Germany) to measure thermal vibration time series at the tip of the microneedle. The incident beam of the interferometer (wavelength $\lambda = 633$ nm; power < 1 mW; ~1 μm spot size) was focused through a 50$\times$ microscope objective and was incident normal to the microneedle as illustrated in Fig. S2 A. The power spectral density of velocity time series was estimated using Welch's periodogram method (49), and the first flexural resonance fitted to a single harmonic oscillator (Fig. S2, B and C). The resulting fitting parameters were used to calculate the stiffness of the microneedle as previously described (48). All calculations were performed in MATLAB version 2013a (The MathWorks, Natick, MA).

Measuring retrograde traction force in growth cones using microneedles

Force-calibrated microneedles were cleaned in piranha solution (H_2SO_4: H_2O_2, 3: 1) for 20 min and rinsed with distilled water five times before incubating the tip in the desired ligand solution for coating. Three different protein ligands were used in this research: 1) 300 μg/ml apCAM in PBS, 2) 100 μg/ml lectin concanavalin A (Con A) (Vector Laboratories, Burlingame, CA) in TBS, or 3) 5 mg/ml bovine serum albumin (BSA) (Sigma-Aldrich, St. Louis, MO) in PBS. We used a three-dimensional (3D)-hydraulic micro-manipulator (Narishige, East Meadow, NY) to position the microneedle onto the growth cone. Contact points were chosen in P domain approximately halfway between the leading edge and the transition zone. Time-lapse differential interference contrast (DIC) imaging was performed using a Nikon TE2000 E2 Eclipse (Nikon, Inc., Melville, NY) inverted microscope equipped with a 60 $\times$ 1.4 oil immersion DIC objective (plus additional 1.5$\times$ magnification) and a Cascade II charge-coupled device camera (Photometrics, Tucson, AZ) controlled by MetaMorph version 7.8.6 (Molecular Devices, Sunnyvale, CA). Images were acquired in 10 s intervals starting immediately after microneedle placement and continued for ~20 min or until the central (C) domain boundary reached the microneedle contact site.

Data analysis

Calculation of retrograde traction force utilizing the AFM *Z* sensor data according to Eq. 14 was performed in MATLAB. Optical images collected during the AFM experiment were processed and analyzed in Image J software (50). For the microneedle experiments, MetaMorph was used for image processing, quantitative analysis of microneedle-growth cone interaction, and retrograde F-actin flow rate measurements. Microneedle deflection was assessed using the object tracking functionality in MetaMorph and confirmed by kymograph analysis. Kymographs were generated from the DIC time-lapse sequences along lines extending from the growth cone leading edge toward the C domain and passing through the microneedle tip. Because of the sharp contrast between the microneedle tip and growth cone features, the microneedle tip appeared as a thick line across kymographs. Retrograde F-actin flow rate was measured by kymograph analysis of DIC time-lapse sequences. Statistical significance was determined using two-tailed unpaired *t*-tests with $\alpha = 0.05$ unless otherwise indicated, using Prism version 6 (GraphPad Software, La Jolla, CA). Graphical illustrations and final figure assembly was performed using Adobe Illustrator version CS6 (Adobe, San Jose, CA) and PowerPoint version 14 (Microsoft, Redmond, WA).

RESULTS

Quantifying traction force generation in growth cones encountering new adhesion substrate with high spatiotemporal resolution

We used two different approaches to measure traction forces with high spatiotemporal resolution as growth cones advance in response to an adhesion substrate in contact with the P domain: 1) AFM and 2) force-calibrated microneedles. In both approaches, the probe (a bead attached to the AFM cantilever tip or the microneedle tip) was brought into contact with the dorsal side of the growth cone P domain and kept in place allowing the growth cone to pull on the force-sensing device. Unlike previous studies using microneedles where external forces were applied on growth cones and axons (4,8,29), in our experiment no towing or any other external force was applied. Fig. 2 *A* shows a complete *Aplysia* neuronal growth cone advance response toward an apCAM-coated bead attached to an AFM cantilever. In this article, the term complete is used to describe growth cone responses when the C domain fully advanced toward and reached the adhesion site. A total of

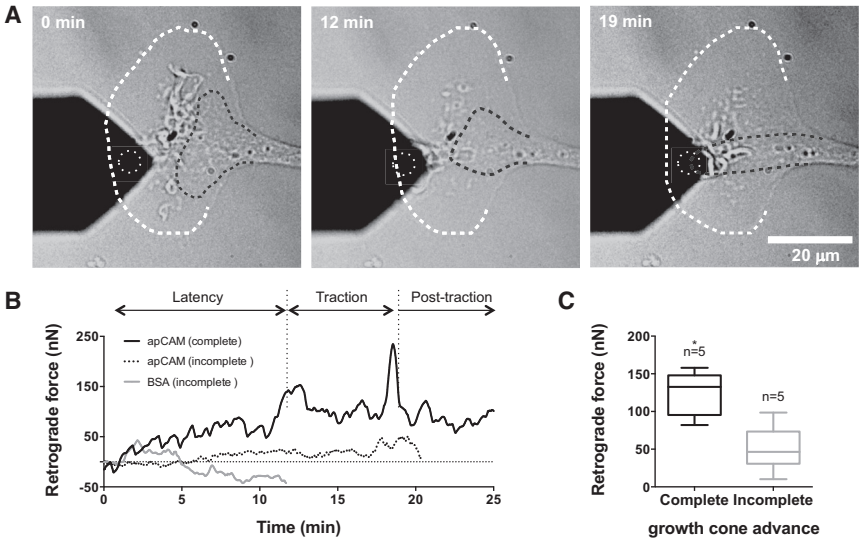

FIGURE 2 Measuring the temporal traction force profile in *Aplysia* growth cones using AFM. (*A*) Phase contrast images showing AFM cantilever modified with apCAM-coated 5 μm bead (*white dashed circle*) interacting with a growth cone at 0, 12, and 19 min following engagement of the cantilever onto the growth cone. C domain boundary (*black dashed line*) started to reorient toward the bead after ~12 min, and reached the bead after 19 min. Leading edge is marked by white dashed line. (*B*) Traction force felt by the apCAM cantilever over time was calculated using Eq. 14. This plot (*solid line*) shows the temporal profile of traction force development in the P domain of the growth cone shown in the sequence of panel (*A*). Also shown are the force profiles for an incomplete growth cone response to an apCAM-coated cantilever (*dotted line*) and a BSA-coated cantilever (*gray line*). (*C*) Comparison of traction force measured at the transition between latency and traction phase for complete interactions and maximum traction force recorded after a corresponding amount of time during incomplete interactions. Box and whiskers plot shows the median, 25th, and 75th percentiles and minimum and maximum values. Asterisk indicates significant difference.

10 AFM experiments were conducted and the probability of a complete growth cone response was 50%. A complete growth cone advance response can be divided into three phases. Following the terminology used in previous work published from our laboratory (42), the first phase is termed latency and extends from time 0 when the cantilever is brought into contact with the growth cone until the C domain boundary starts to reorient toward the apCAM bead. This phase involves adhesion formation, Src tyrosine phosphorylation, and early microtubule exploration of the adhesion site (13,40,42). The second phase is termed traction, which starts at the end of latency and ends when the C domain reaches the adhesion site. This phase involves major cytoskeletal and cytoplasmic domain rearrangements, actin flow reduction, traction force buildup, and leading edge growth (13,42,43). We also define the third or posttraction phase, during which the C domain becomes strongly attached to the bead, and relatively violent fluctuations of the apCAM bead are often observed.

Traction force generation over time as the growth cone interacted with the apCAM-coated colloidal AFM cantilever is shown in Fig. 2 *B*. Traction force in the retrograde direction increased gradually during the 12 min latency period up to 100 nN and peaked at the end of the traction period as the C domain reached the apCAM bead. At that point, the C domain pushed the cantilever in the anterograde direction, thus reducing the net retrograde force felt by the cantilever. Control BSA-coated AFM cantilever did not elicit C domain advance or traction force development (Fig. 2 *B*). Similarly, when the growth cones did not respond completely to apCAM-coated cantilevers, traction force remained significantly lower. Traction force measured at the transition from latency into traction phase was 123.9 $\pm$ 13.1 nN (n = 5; mean value $\pm$ SE; Fig. 2 *C*) in the case of complete growth cone advance. For incomplete growth cone responses, the maximum force during the time of experiment (~20 min) was significantly lower at 50.7 $\pm$ 12.1 nN (n = 5; Fig. 2 *C*). As shown in Fig. S3, whereas force gradually increased in all observed advance responses, the temporal profile varied between different growth cones.

To confirm our AFM data, we measured traction force using force-calibrated microneedles. A typical complete growth cone response to an apCAM-coated microneedle is shown in Fig. 3 *A* at three different time points: beginning of latency (*left*), end of latency (*middle*), and end of traction phase (*right*) (see also Movie S1). Traction force was generated through coupling of the apCAM-coated microneedle to the underlying retrograde actin flow, which causes the microneedle to deflect in the retrograde direction. A kymograph of needle position shows initial negative force likely caused by increased ruffling activity at the contact site (Fig. 3 *B*). Similar ruffling activity was previously observed along with increased actin assembly around mechanically restrained apCAM-coated beads in experiments with *Aplysia* growth cones (13,34,51). After an initial ruffling push, the growth cone started to pull the microneedle in the retrograde direction as seen in the kymograph in Fig. 3 *B*. By measuring microneedle deflection, traction force F is calculated using Hooke's law $F = kx$, where k is the stiffness of the microneedle and x is microneedle deflection (Fig. 3 *C*). In the example shown, traction force increased at the end of the latency phase while retrograde actin flow rate decreased, consistent with gradually increasing coupling between the apCAM-coated microneedle and the actin retrograde flow (Fig. 3 *C*). Reduction of retrograde actin flow at the end of the latency phase and beginning of the traction phase is consistent with our previous observations (13,42).

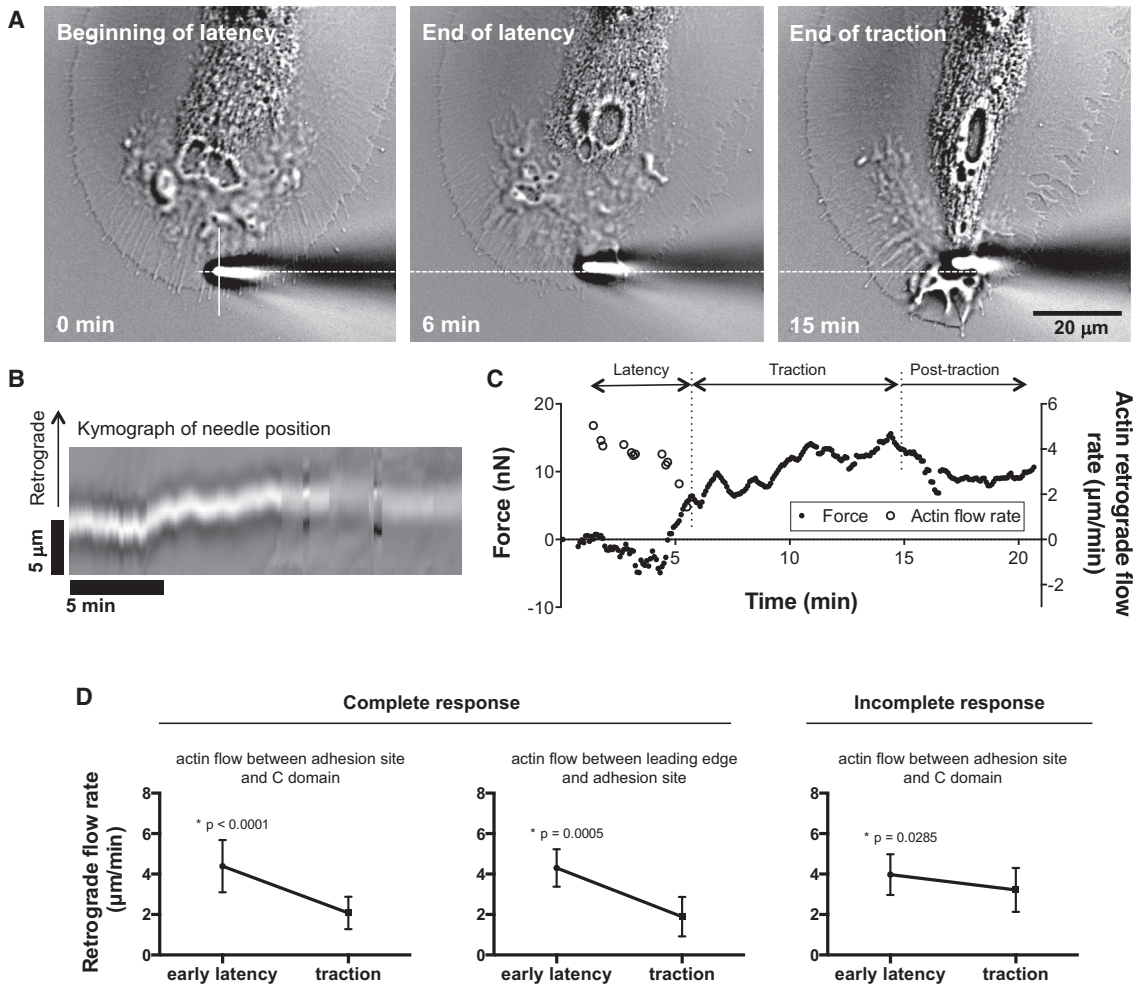

FIGURE 3 Growth cone traction force measured by apCAM microneedles. (*A*) DIC images showing an apCAM-coated microneedle with 0.007 N/m stiffness interacting with a growth cone. The three images show the microneedle when first touching the growth cone (0 min), the C domain beginning reorientation toward the microneedle contact point (6 min; end of latency period), and C domain reaching the microneedle tip (15 min; end of traction period). (*B*) Kymograph taken along the white line in (*A*) and showing the position of the microneedle throughout the time course of the growth cone response. (*C*) Retrograde force exerted by the growth cone on the microneedle over time (*solid circles*) and F-actin retrograde flow rate during latency (*open circles*). (*D*) Comparison of F-actin retrograde flow rates for complete and incomplete growth cone responses early in latency and traction periods, respectively. Middle graph shows flow rates measured between the leading edge and the needle tip, whereas left and right graphs show flow rates measured between the needle tip and the C domain. Mean values ± SE; paired *t*-test.

Traction force continued to increase during traction phase and peaked at 15.6 nN just before the C domain reached the adhesion site in the example shown in Fig. 3 *A*. The C domain pushed the microneedle in the posttraction phase causing a decrease in net traction force exerted on the microneedle. The temporal profiles of traction force for several apCAM and Con A needle experiments are shown in Figs. S4 and S5 and Movies S1 and S2, respectively. As observed with the AFM approach (Fig. S3), the profile of the force development varied between individual growth cones.

Analysis of actin retrograde flow in all complete microneedle experiments showed a 53% (n = 22) reduction in actin flow rate in the area between the microneedle and the C domain and 56% (n = 22) reduction in flow rate in the advancing lamellipodia between the leading edge and the microneedle (Fig. 3 *D*). This is the first time that we measured flow rates between the advancing leading edge and the adhesion site in addition to the area between the adhesion site and the C domain. The flow reduction on either side of the needle tip strongly suggests that a large retrogradely flowing actin network was physically coupled to the microneedle beyond the immediate adhesion site. For experiments with incomplete growth cone responses, a statistically significant reduction in actin flow rate was also observed, although the 19% (n = 20) reduction was not as severe as in the case of complete responses (Fig. 3 *D*). In summary, we observed that growth cones gradually build up traction force during latency and traction phases, whereas retrograde actin flow significantly slows down at the end of latency.

Traction force correlates with microneedle stiffness

Although we initially attempted to produce microneedles of identical stiffness, the microneedles used in our experiments showed variation. A trend was emerging that stiffer microneedles resulted in higher traction force values. Therefore, we tested the hypothesis that traction force correlates with the stiffness of the microneedle. Fig. 4 shows strong correlation between microneedle stiffness and traction force observed immediately before the C domain advanced toward the microneedle. We conducted experiments with apCAM- and Con A-coated microneedles; both are adhesion proteins that bind the cell surface apCAM (13). Both substrates show a significant higher response probability compared with BSA-coated or uncoated microneedles used as negative controls (Table 1). Correlation between traction force and needle stiffness was high for both apCAM ($R^2 = 0.81$) and Con A ($R^2 = 0.85$) needles. Interestingly, the slope of the best-fit line was higher for apCAM, suggesting that apCAM substrate may be a more specific force transmitter than Con A. apCAM is a homophilic cell adhesion molecule, whereas Con A binds apCAM among other proteins (52,53).

Substrate deformation and not traction force predicts growth cone advance

As shown above, we have found that the amount of traction force produced by the growth cone strongly depends on the stiffness of the microneedle. We were interested to determine whether there was a certain threshold force needed to induce complete growth cone advance. A comparison of measured traction force values of all complete and incomplete microneedle experiments revealed that the magnitude of force exerted by the growth cone on the microneedle does not predict whether the growth cone will advance in the direction of the adhesion protein-coated microneedle or not. Although, traction forces at the end of the latency period for complete growth cone advance responses to apCAM-microneedles were generally larger than in the case of incomplete interactions, the difference was not statistically significant ($p = 0.104$ for apCAM and $p = 0.730$ for Con A; Fig. 5 *A*). It was evident that the magnitude of

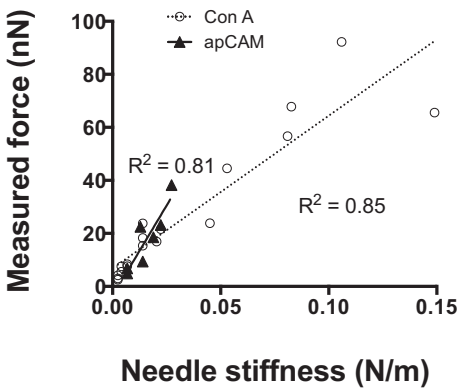

FIGURE 4 Measured force is proportional to microneedle stiffness. Relationship between traction force measured immediately before the C domain advanced toward the microneedle and the stiffness of the microneedle used to perform the measurement. Separate correlations are shown for apCAM- and Con A-coated microneedles.

TABLE 1 Summary of all microneedle experiments

	Con A	apCAM	BSA	Uncoated
Number of experiments	33	28	12	17
Number of complete responses	19	9	1	2
% complete responses	58	32	8	12
Average latency length (min)	8.2 (± 1.4)	10.1 (± 1.6)		

Con A, concanavalin A; apCAM, *Aplysia* cell adhesion molecule; BSA, bovine serum albumin.

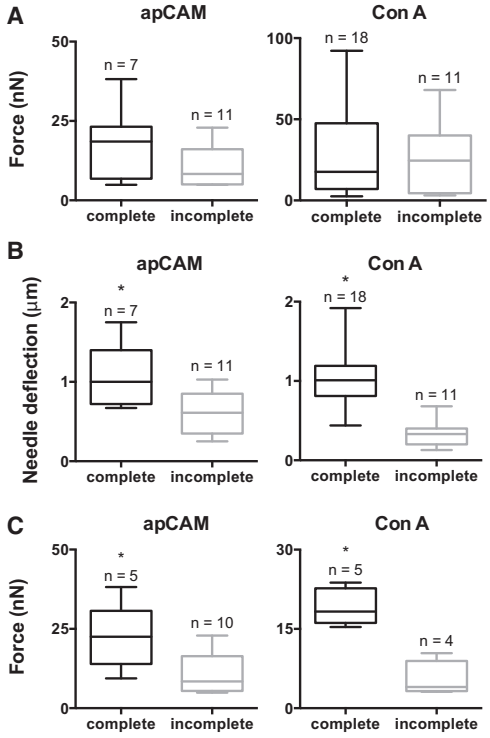

FIGURE 5 Microneedle deflection is a better predictor of growth cone advance than absolute traction force values. (*A*) Comparison of force measured for complete and incomplete growth cone responses for apCAM and Con A microneedles. For incomplete growth cone response, the value reported is the maximum force value within 10 min from the time the microneedle was lowered onto the growth cone, which corresponds to the mean latency time of apCAM-induced responses. (*B*) Comparison of microneedle deflection observed for complete and incomplete growth cone responses for apCAM and Con A microneedles, respectively. (*C*) Comparison of traction force measured for complete and incomplete growth cone responses using microneedles with a very narrow range of stiffness (0.018 ± 0.001 N/m, n = 24). Box and whiskers plots show the median, 25th and 75th percentiles, and minimum and maximum values. Asterisk indicates significant difference.

traction force by itself does not determine whether the growth cone will undergo a complete response or not. For instance, some growth cones advanced after exerting forces as low as 2.5 nN and as high as 92.2 nN, depending on the microneedle stiffness, whereas other growth cones did not advance despite exerting forces as high as 68 nN.

By contrast, the magnitude of microneedle deflection (i.e., adhesion substrate deformation) appears to be a better predictor of whether the growth cone will advance in the direction of the adhesion substrate or not (Fig. 5 *B*). In cases of complete growth cone advance, the mean microneedle deflection at the end of the latency period was 1.08 ± 0.14 (n = 7) and 1.04 ± 0.09 (n = 18) μm for apCAM and Con A microneedles, respectively. These values were significantly higher ($p = 0.008$ for apCAM and $p < 0.0001$ for Con A; Fig. 5 *B*) than in cases of incomplete responses to both apCAM and Con A microneedles where deflection remained below 0.62 ± 0.08 (n = 11) and 0.33 ± 0.05 (n = 11) μm, respectively. However, when we compared traction force generation in complete and incomplete growth cone responses using microneedles within a very narrow range of stiffness, we noticed a significant difference in mean traction force values ($p = 0.018$ for apCAM and $p = 0.001$ for Con A; Fig. 5 *C*), which is also in agreement with our findings using AFM cantilevers of similar stiffness (Fig. 2 *C*). This shows that a certain force value can only be an indicator of complete advance response for specific substrate stiffness.

To further confirm the correlation of growth cone advance response with substrate deformation as opposed to the level of traction force, we sequentially probed the same growth cone with two microneedles of different stiffness. In the experiment shown in Fig. 6, a growth cone was first probed by a Con A-coated microneedle with 0.0025 N/m stiffness (Fig. 6 *A*). Con A was used in this experiment because the probability of a complete response was higher with Con A than with apCAM microneedles (Table 1). After observing a complete growth cone advance response, the microneedle was carefully disengaged to prevent damage to the growth cone. The growth cone was allowed to recover for ~15 min before another Con A-coated microneedle with 0.014 N/m stiffness was placed on the growth cone and another complete response was observed (Fig. 6 *B*). Although the growth cone responded to both microneedles, measured traction force at the end of latency was proportional to microneedle stiffness (3.0 vs. 15.4 nN). Interestingly, the observed microneedle deflection at the end of latency was virtually the same (1.11 vs. 1.05 μm). This experiment was repeated three times using different cells and similar results were obtained each time, independently of the order of needle application (Figs. S6 and S7). In summary, we observed that individual growth cones can produce a wide range of traction forces during adhesion-mediated growth cone advance, the level of which is correlated to the substrate (i.e., microneedle) stiffness. These results suggest that with respect to advance or not, the growth cone is more sensitive to the amount of substrate deformation than to the magnitude of traction force.

DISCUSSION

Quantification of traction force generation during adhesion-mediated growth cone advance

To fully understand the mechanism of force generation and transmission in the growth cone as well as its role in axonal growth and guidance, it is critical to have quantitative information about the relationships between forces, cytoskeletal dynamics, molecular motors, biochemical signaling, substrate adhesion, and stiffness, which all contribute to directional growth cone advance. In this study, we have measured traction force as it develops in the growth cone during adhesion-mediated advance with unprecedented spatial and temporal resolution. Although growth cone traction forces have been previously quantified using different experimental techniques, our study is the first, to our knowledge, to quantify the development of traction forces as the growth cone is actively responding to a change in molecular and mechanical stimuli.

Among the different methods for studying forces in neurons, microneedles were used first by the groups of Bray and Heidemann more than two decades ago. These studies provided a global view of mechanical forces at the whole neuron and neurite level as opposed to local growth cone traction force. The first force measurements using force-calibrated microneedles were performed by Heidemann and co-workers in PC-12 neurites, which were found to be under permanent mechanical tension, so-called rest tension, ranging over three orders of magnitude (10^{-2} to 10^{0} nN) (8). The same group later presented the first direct evidence that growth cones pull by generating traction force (4). A force-calibrated microneedle was attached to the soma of a cultured chick sensory neuron and raised so that the cell became attached to the substrate at the growth cone only. Neurite tension was found to be in the 10^{0} nN range and strongly correlated to growth cone advance (4). Saif and co-worker (6,36) fabricated a silicon-based micromechanical force sensor to measure rest tension in the axons of *Drosophila* neurons in vivo and found it to be in the 10^{0} to 10^{1} nN range. Recently, O'Toole et al. (29) presented a mathematical model describing the relationship between subcellular forces arranged in series within the axon and the net axonal tension. They elegantly combined the use of force-calibrated microneedle to measure and apply force with labeling of docked mitochondria to monitor subcellular strain in chick sensory neurons. Based on experimental results and the model, the mean forces were found to be 2.0 and 0.6 nN at the rear of the growth cone and axon, respectively. In contrast to all these previous studies, the

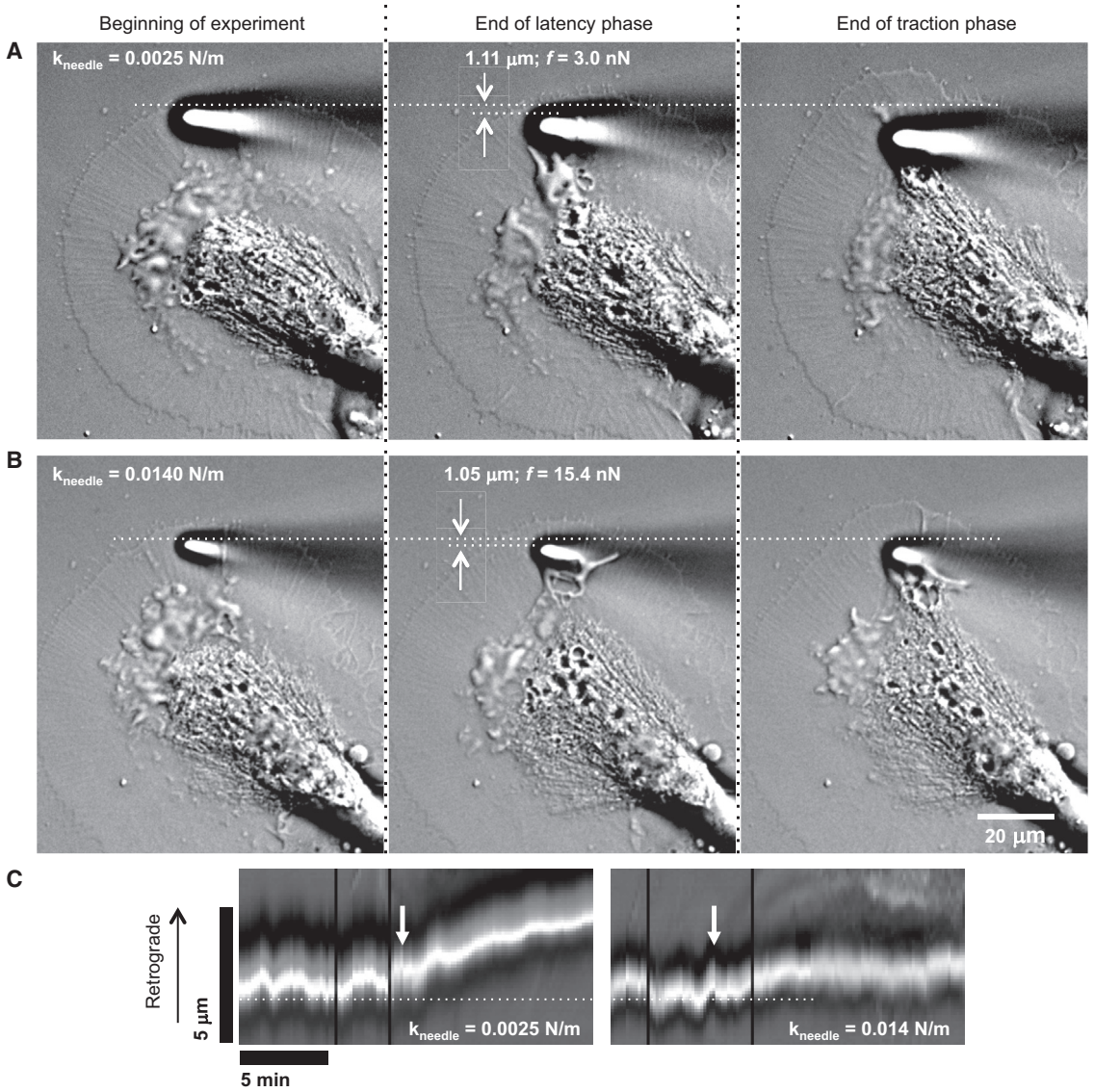

FIGURE 6 The same growth cone produces different amounts of traction force during adhesion-mediated advance. (*A*) DIC images of a growth cone interacting with a 0.0025 N/m Con A-coated microneedle at the beginning of the experiment, at the end of latency and traction phases. (*B*) The same growth cone shown in (*A*) interacting with 0.0140 N/m Con A-coated microneedle. Needle stiffness (k), needle deflection, and traction force are indicated. (*C*) Kymographs showing the position of the microneedle throughout the time course of the experiments shown in (*A*) and (*B*). Arrows indicate the end of latency phase.

microneedle in our experiments interacted with the growth cone specifically in the P domain, and no towing was introduced. Therefore, the needles used in our approach measured traction force solely as the result of the growth cone interacting with the microneedle.

Traction force microscopy with flexible substrates was used to measure forces generated by filopodia in growth cones from superior cervical ganglion neurons (14). Peak traction forces were in the 10^0 nN range. Using the same technique, Hyland et al. (20) found that *Aplysia* growth cones generate traction force on the order of 10^0 nN, which is consistent with some of our data revealing forces as low as 3 nN during adhesion-mediated growth cone advance. Using flexible substrates, Koch et al. (19) found that the growth cones of peripheral neurons produce higher traction forces compared with central nervous systems neurons (10^0 vs. 10^{-1} nN range). Hällström et al. (31) used nanowire arrays and measured traction forces in the 10^{-2} to 10^1 nN range exerted by the growth cones of rat dorsal root ganglion neurons, depending on the stiffness of the nanowires. Whereas traction force microscopy provides quantitative information at the growth cone level, it is critical to note that these measurements are performed while the growth cone is growing on a molecularly and mechanically uniform substrate. Our experimental approach is different from previous studies in that traction force was measured during an active growth

cone response to a molecular and mechanical change of the adhesion substrate. The strong local coupling between the actin network and the apCAM-coated AFM cantilever or the microneedle triggered a distinct response pattern involving major rearrangements of cytoplasmic domains and cytoskeletal structures (Figs. 2 *A* and 3 *A*) consistent with our previous results using a mechanically restrained apCAM-coated microbead (13,40,42).

Using optical tweezers, the forces exerted by the filopodia and lamellipodia of rat hippocampal and dorsal root ganglia were found to be on the order of 10^{-3} and 10^{-2} nN, respectively (33). Furthermore, the strength of elastic coupling of apCAM adhesions to actin flow in *Aplysia* growth cones was on the order of 10^{-2} nN as determined by optical tweezers (34). Whereas the optical tweezers approach circumvents the issue of substrate uniformity, the level of force that can be applied with optical and magnetic tweezers to the cell without causing damage is typically below the threshold required to induce adhesion-mediated growth cone advance. Lastly, AFM was used to quantify forward pushing forces of mouse retinal ganglion cell and NG108-15 growth cones (35). Using lateral force microscopy, peak forward pushing in addition to retrograde forces were found to be on the order of 10^{-1} nN (35). Although lateral force microscopy appears to be an ideal solution for measuring traction force in growth cones, significant technical difficulties exist particularly related to calibrating the torsional response of the AFM cantilever (45). Accordingly, we built on the work of Karhu et al. (45) and developed a new approach, to our knowledge, for measuring retrograde force by monitoring the vertical height of the AFM cantilever as it interacts with the growth cone. With the new method, we were able to measure horizontal forces exerted on the AFM cantilever without the need to perform lateral force calibration. In summary, our approach to determine traction force during adhesion-mediated growth cone advance is clearly distinct from previous studies that reported on forces that (1) involved larger regions of the neuron (2), were developed by growth cones interacting with uniform substrates, or (3) reflected local substrate-cytoskeletal coupling events that were insufficient to induce adhesion-mediated growth cone advance.

Traction force gradually increases during adhesion-mediated growth cone advance

Both AFM and microneedle measurements showed that traction force in the P domain gradually increased over time during adhesion-mediated growth as coupling got stronger during latency. Force further increased during the traction phase, when major cytoskeletal reorganizations occur, and peaked just before the C domain reached the needle (Figs. 2, 3, and S3–S5). Gradual force increase was matched by gradual decrease in retrograde actin flow, which supports the substrate-cytoskeletal coupling model (22) and is consistent with previous observations made using the RBI assay (13,42–44), although in those experiments force measurements were not performed. Whereas noticeable actin flow reduction typically occurred late in latency as seen in Fig. 3 *C* and previous studies (13,42), we observed frequently gradual buildup of traction force earlier in latency using both force measuring approaches (Figs. S3–S5). This early raise in traction force before significant flow attenuation occurred could reflect the gradual buildup of engaged clutches.

We measured traction forces during complete growth cone advance responses ranging over two orders of magnitudes. Although we observed traction forces in the 10^{0} to 10^{1} nN range similar to previous studies (19,20,29,31), we are the first, to our knowledge, to report growth cone forces up in the 10^{2} nN range. Considering the large size and cytoskeletal mass of *Aplysia* growth cones such high force levels may not be surprising. However, it is important to point out that a direct comparison with previous studies can be problematic because 1) reported force values are not necessarily analogous, and 2) contact area, molecular, and mechanical properties of the sampling probe usually vary among different studies. For example, we and others have observed a positive correlation between substrate stiffness and measured force (19,54–58). Although both AFM and microneedle methods revealed traction forces in *Aplysia* growth cones in a similar range, directly comparing force values measured by AFM and microneedles is challenging for a number of reasons: 1) knowing the effective cantilever stiffness is difficult, 2) the AFM experiment was performed with the feedback loop turned on to satisfy Eq. 9, and 3) because the calculation of traction force using our AFM approach depends on changes in cantilever height (Eq. 14), the accuracy of measurement is influenced by any factor that causes a change in cantilever height other than traction force. For example, an increase in growth cone thickness because of cytoskeletal rearrangements during the growth cone interaction with the cantilever tip could inflate the traction force value calculated. Because we are currently unable to determine such potential height changes independently from traction forces, it was important that we measured traction force using two completely independent experimental approaches, AFM and force-calibrated microneedles. Force values derived from the AFM approach were generally higher than force values determined with microneedles, which may indicate that height changes because of cytoskeletal remodeling caused an overestimate. The microneedle approach is insensitive to potential growth cone height changes but could potentially suffer from systematic drift in the position of microneedle tip relative to the growth cone. Initially, we attempted to include a second reference microneedle mounted on the same holder to account for drift, but that proved to be challenging given our setup and the very small field of view under 60× objective. However, control experiments with microneedles raised slightly above the surface were conducted to make sure drift was not

influencing the position of the microneedle. Additionally, we alternated the orientation of growth cones to account for any potential systematic drift. In about half of the experiments, the growth cone was oriented such that the axis from the central domain to the microneedle tip was pointing upward, whereas for the other half of experiments, that axis was pointing downward.

In summary, despite potential inaccuracies in the true force values, the two independent measurements techniques showed that traction force increases steadily throughout the latency period. This novel observation, to our knowledge, is particularly intriguing and raises questions about the mechanisms and signaling cascades involved in, and influenced by, force build up in the growth cone cytoskeletal network.

The growth cone advance response correlates with substrate deformation

Somewhat unexpectedly, we did not identify a threshold force level that would be required for a complete advance response. Interestingly, growth cone advance responses correlated with the level of microneedle deflection and less so with the magnitude of force (Fig. 5). We confirmed this relationship by probing the same growth cone twice using two microneedles of different stiffness. We repeated this experiment with three different cells, and in each case, traction force at the end of the latency phase was proportional to the microneedle stiffness; however, microneedle deflection was 1.2 $\pm$ 0.1 μm (Figs. 6, S6, and S7). Such a correlation between substrate stiffness and mechanical response by the cell is in agreement with previous studies. Choquet et al. (54) showed that the strength of substrate-cytoskeletal coupling in the lamellipodia of mouse fibroblasts increased proportionally with substrate rigidity. A similar cellular reinforcement behavior was observed in studies with epithelial cells (55,56) and fibroblasts (56–58). Using traction force microscopy, Koch et al. (19) showed that forces generated by dorsal root ganglia and hippocampal growth cones both increase with increasing substrate stiffness. Our results are in agreement with these findings and suggest a cellular reinforcement mechanism that responds to the extracellular stiffness. What is the underlying mechanism and the role of reinforcement? A positive feedback loop system between tyrosine phosphorylation and tension development could provide an answer to the first question (40). Whether cells use the reinforcement mechanism to decide in which direction they migrate is an interesting hypothesis. There is evidence that migrating cells decide in which direction to advance partly by sensing and responding to the stiffness of the extracellular matrix (19,59–62). However, whether the cellular response is governed by force (stress) or deformation (strain) or both has remained unclear (55–58,63). Our results show that the magnitude of traction force itself is not a good predictor of the growth cone advance response (Fig. 5, *A* and *B*). By comparison, the level of microneedle deflection better predicts whether the growth cone will advance toward the adhesion site or not (Fig. 5, *A* and *B*). Within the boundaries of our experiment, our results suggest that substrate deformation is a more relevant factor in determining a cellular response.

Mechanosensing involves cytoskeletal structures beyond immediate adhesion site

Different molecular mechanisms have been proposed to explain force sensing by cells, including stretch-activated ion channels and conformational changes in proteins regulating tyrosine phosphorylation (62). Stretch-activated calcium channels mediate neurite retraction in NG108-15 and PC12 cells, which requires a stress threshold (23). Although stretch-activated molecular structures provide a plausible mechanism for sensing mechanical stress, they alone do not explain the extent of the constant micron-scale substrate deformations. Our results support a mechanosensing mechanism that involves structural elements spanning a micron-scale distance. The mean microneedle deflection was 1.05 $\pm$ 0.07 μm when the growth cones advanced in the direction of the adhesion site for both Con A and apCAM microneedles. By contrast, the mean deflection was significantly lower (0.48 $\pm$ 0.06 μm) when the growth cones did not respond to the adhesion substrate. Interestingly, Trichet et al. (57) observed a constant deformation of the substrate of around 0.84 $\pm$ 0.03 μm caused by migrating fibroblasts. The relatively large deformations we and others observed imply a mechanosensing mechanism that involves structures spanning a large spatial range such as actin and microtubule cytoskeleton and not only local protein interactions at the adhesion site, such as stretch-induced phosphorylation or opening of ionic channels. This conclusion is also supported by our analysis of retrograde actin flow rate, which showed a 53% reduction in the area between the microneedle and the C domain and 56% reduction in the area between the leading edge and the microneedle (Fig. 3 *D*), suggesting a larger area of the flowing actin network beyond the immediate adhesion site was physically coupled to the microneedle. In support of this idea, Mejean et al. (34) recently reported that the mechanical properties of nascent apCAM-mediated adhesions in *Aplysia* growth cones were dominated by elastic structures that undergo micron-sized reversible deformations, suggesting the substrate was physically coupled to a large cross-linked actin network beyond the immediate adhesion site. Furthermore, Trichet et al. (57) argue convincingly that the fact that stress applied by the cell depends on substrate stiffness provides direct evidence that a feedback involving structures other than focal adhesions must be involved (57).

The micron-scale deformation of nascent apCAM-mediated adhesions observed by Mejean et al. (34) occurred over 15 s, whereas the micron-scale substrate deformation we and Trichet et al. (57) observed occurred over 15 to

20 min, during which traction force grew steadily. Are these two sets of observations, which occurred over different timescales, related? And, if so, how? How is cellular movement related to the observed substrate deformation, which averages around 1 μm? One possible explanation could be that the observed substrate deformation, which correlates with growth cone advance response, is related to the maximum length to which nascent actin-based adhesion structures can be stretched before they break (Fig. 7). Adhesions form and break on a timescale of seconds, but the resultant effect is felt by the microneedle as a permanent linkage. That linkage grows stronger as adhesion become more abundant and more are forming than breaking.

The growth cone, including the microtubule- and organelle-rich C domain, advances when F-actin flow in the P domain is significantly slowed down. For this to happen, substrate-cytoskeletal linkage involving growing actin filaments (also referred to as elastic nascent adhesions) must be strong enough to bear the building tension. When the linkage is strong enough, it holds without breaking at the maximum extendable length, which appears to be on the order of 1 μm (Fig. 7). Although nascent adhesions are dynamic and transient, over time they become more abundant and capable of bearing increasing tension. This was evident in the experiment by Trichet et al. (57), which showed steady growth of focal adhesion area with time. Taken together, we propose a hypothesis according to which nascent adhesions may be considered as individual rubber bands, each can undergo micron-scale deformation (Fig. 7). Early during the latency period, they break because individually they cannot hold the connection between the microneedle tip and the flowing actin network. However with time, more rubber bands are recruited. The resultant effect of this dynamic coupling is a temporal increase in the force transiently felt by the microneedle tip. Once the number of rubber bands is high enough, the connection is held extended and actin flow is reduced to a halt, thus initiating the growth cone advance mechanism.

In summary, we believe that the micron-scale deformation observed in our and other studies, are related to the elasticity of actin-based adhesion structures forming between the substrate and the flowing actomyosin network. Although it is still unclear whether this seemingly constant micron-scale substrate deformation is of physiological significance (e.g., having a regulatory role), our findings suggest a stiffness-sensitive mechanism that likely involves cytoskeletal elements spanning a large spatial range that goes beyond local interactions at the adhesion site.

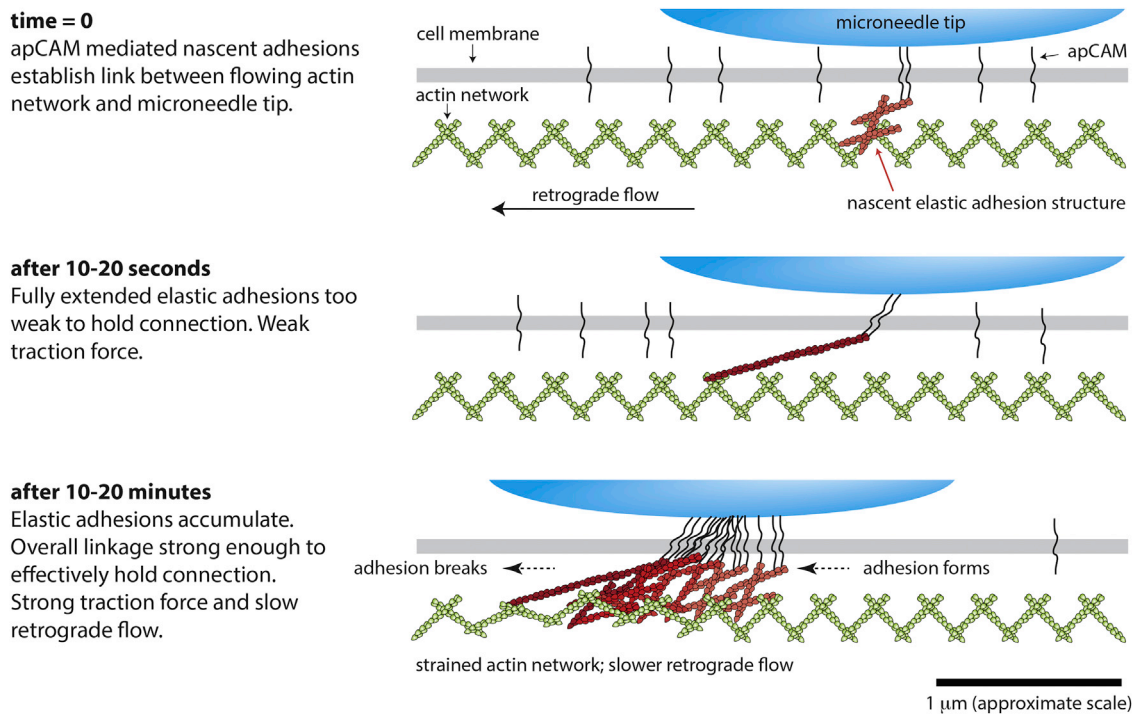

FIGURE 7 Hypothesis: development of traction force and the origin of the observed micrometer-scale substrate (microneedle) deformation. Upon contact with the microneedle tip, the nascent apCAM-mediated actin-based elastic adhesions establish linkage between the flowing actin network and microneedle tip. Individually, elastic adhesions are too weak to hold the connection, resulting in a very low traction force. Over time, dynamic and transient adhesions become more abundant and capable of bearing increasing tension, resulting in higher traction force and reduced retrograde flow. The magnitude of microneedle tip movement is related to the micrometer scale length to which elastic adhesions can be stretched before breaking (34). To see this figure in color, go online.

SUPPORTING MATERIAL

Seven figures and two movies are available at http://www.biophysj.org/biophysj/supplemental/S0006-3495(15)00824-3.

AUTHOR CONTRIBUTIONS

A.A. and D.S. designed experiments; A.A. and A.C. performed experiments; A.A., A.C., and A.R. contributed analytic tools; A.A., A.C., A.R., and D.S. analyzed data; and A.A. and D.S. wrote the article.

ACKNOWLEDGMENTS

We thank Nurul H. Shaik from the laboratory of Dr. Raman for training on using a laser Doppler vibrometer (LDV) and analyzing LDV data. We are grateful to the National Science Foundation for support of this work under Grant No. 1146944-IOS.

REFERENCES

1. Suter, D. M., and K. E. Miller. 2011. The emerging role of forces in axonal elongation. *Prog. Neurobiol.* 94:91–101.
2. Franze, K., P. A. Janmey, and J. Guck. 2013. Mechanics in neuronal development and repair. *Annu. Rev. Biomed. Eng.* 15:227–251.
3. Bray, D. 1979. Mechanical tension produced by nerve cells in tissue culture. *J. Cell Sci.* 37:391–410.
4. Lamoureux, P., R. E. Buxbaum, and S. R. Heidemann. 1989. Direct evidence that growth cones pull. *Nature.* 340:159–162.
5. Heidemann, S. R., P. Lamoureux, and R. E. Buxbaum. 1990. Growth cone behavior and production of traction force. *J. Cell Biol.* 111:1949–1957.
6. Rajagopalan, J., A. Tofangchi, and M. T. A Saif. 2010. Drosophila neurons actively regulate axonal tension in vivo. *Biophys. J.* 99:3208–3215.
7. Bray, D. 1984. Axonal growth in response to experimentally applied mechanical tension. *Dev. Biol.* 102:379–389.
8. Dennerll, T. J., H. C. Joshi, …, S. R. Heidemann. 1988. Tension and compression in the cytoskeleton of PC-12 neurites. II: quantitative measurements. *J. Cell Biol.* 107:665–674.
9. Dennerll, T. J., P. Lamoureux, …, S. R. Heidemann. 1989. The cytomechanics of axonal elongation and retraction. *J. Cell Biol.* 109:3073–3083.
10. Gilmour, D., H. Knaut, …, C. Nüsslein-Volhard. 2004. Towing of sensory axons by their migrating target cells in vivo. *Nat. Neurosci.* 7:491–492.
11. Chan, C. E., and D. J. Odde. 2008. Traction dynamics of filopodia on compliant substrates. *Science.* 322:1687–1691.
12. Lin, C. H., E. M. Espreafico, …, P. Forscher. 1996. Myosin drives retrograde F-actin flow in neuronal growth cones. *Neuron.* 16:769–782.
13. Suter, D. M., L. D. Errante, …, P. Forscher. 1998. The Ig superfamily cell adhesion molecule, apCAM, mediates growth cone steering by substrate-cytoskeletal coupling. *J. Cell Biol.* 141:227–240.
14. Bridgman, P. C., S. Dave, …, R. S. Adelstein. 2001. Myosin IIB is required for growth cone motility. *J. Neurosci.* 21:6159–6169.
15. Turney, S. G., and P. C. Bridgman. 2005. Laminin stimulates and guides axonal outgrowth via growth cone myosin II activity. *Nat. Neurosci.* 8:717–719.
16. Bard, L., C. Boscher, …, O. Thoumine. 2008. A molecular clutch between the actin flow and N-cadherin adhesions drives growth cone migration. *J. Neurosci.* 28:5879–5890.
17. Shimada, T., M. Toriyama, …, N. Inagaki. 2008. Shootin1 interacts with actin retrograde flow and L1-CAM to promote axon outgrowth. *J. Cell Biol.* 181:817–829.
18. Betz, T., D. Koch, …, J. A. Käs. 2011. Growth cones as soft and weak force generators. *Proc. Natl. Acad. Sci. USA.* 108:13420–13425.
19. Koch, D., W. J. Rosoff, …, J. S. Urbach. 2012. Strength in the periphery: growth cone biomechanics and substrate rigidity response in peripheral and central nervous system neurons. *Biophys. J.* 102:452–460.
20. Hyland, C., A. F. Mertz, …, E. Dufresne. 2014. Dynamic peripheral traction forces balance stable neurite tension in regenerating *Aplysia* bag cell neurons. *Sci. Rep.* 4:4961.
21. Lin, C.-H., and P. Forscher. 1995. Growth cone advance is inversely proportional to retrograde F-actin flow. *Neuron.* 14:763–771.
22. Suter, D. M., and P. Forscher. 2000. Substrate-cytoskeletal coupling as a mechanism for the regulation of growth cone motility and guidance. *J. Neurobiol.* 44:97–113.
23. Franze, K., J. Gerdelmann, …, J. Käs. 2009. Neurite branch retraction is caused by a threshold-dependent mechanical impact. *Biophys. J.* 97:1883–1890.
24. Kerstein, P. C., B. T. Jacques-Fricke, …, T. M. Gomez. 2013. Mechanosensitive TRPC1 channels promote calpain proteolysis of talin to regulate spinal axon outgrowth. *J. Neurosci.* 33:273–285.
25. Rajnicek, A., and C. McCaig. 1997. Guidance of CNS growth cones by substratum grooves and ridges: effects of inhibitors of the cytoskeleton, calcium channels and signal transduction pathways. *J. Cell Sci.* 110:2915–2924.
26. Gomez, T. M., E. Robles, …, N. C. Spitzer. 2001. Filopodial calcium transients promote substrate-dependent growth cone turning. *Science.* 291:1983–1987.
27. Lamoureux, P., J. Zheng, …, S. R. Heidemann. 1992. A cytomechanical investigation of neurite growth on different culture surfaces. *J. Cell Biol.* 118:655–661.
28. Chada, S., P. Lamoureux, …, S. R. Heidemann. 1997. Cytomechanics of neurite outgrowth from chick brain neurons. *J. Cell Sci.* 110:1179–1186.
29. O'Toole, M., P. Lamoureux, and K. E. Miller. 2015. Measurement of subcellular force generation in neurons. *Biophys. J.* 108:1027–1037.
30. Toriyama, M., S. Kozawa, …, N. Inagaki. 2013. Conversion of a signal into forces for axon outgrowth through Pak1-mediated shootin1 phosphorylation. *Curr. Biol.* 23:529–534.
31. Hällström, W., M. Lexholm, …, C. N. Prinz. 2010. Fifteen-piconewton force detection from neural growth cones using nanowire arrays. *Nano Lett.* 10:782–787.
32. Shahapure, R., F. Difato, …, V. Torre. 2010. Force generation in lamellipodia is a probabilistic process with fast growth and retraction events. *Biophys. J.* 98:979–988.
33. Amin, L., E. Ercolini, …, V. Torre. 2013. Comparison of the force exerted by hippocampal and DRG growth cones. *PLoS One.* 8:e73025.
34. Mejean, C. O., A. W. Schaefer, …, P. Forscher. 2013. Elastic coupling of nascent apCAM adhesions to flowing actin networks. *PLoS One.* 8:e73389.
35. Fuhs, T., L. Reuter, …, J. A. Käs. 2013. Inherently slow and weak forward forces of neuronal growth cones measured by a drift-stabilized atomic force microscope. *Cytoskeleton (Hoboken).* 70:44–53.
36. Siechen, S., S. Yang, …, T. Saif. 2009. Mechanical tension contributes to clustering of neurotransmitter vesicles at presynaptic terminals. *Proc. Natl. Acad. Sci. USA.* 106:12611–12616.
37. Zheng, J., R. E. Buxbaum, and S. R. Heidemann. 1994. Measurements of growth cone adhesion to culture surfaces by micromanipulation. *J. Cell Biol.* 127:2049–2060.
38. Bernal, R., P. A. Pullarkat, and F. Melo. 2007. Mechanical properties of axons. *Phys. Rev. Lett.* 99:018301.
39. Moore, S. W., N. Biais, and M. P. Sheetz. 2009. Traction on immobilized netrin-1 is sufficient to reorient axons. *Science.* 325:166.

40. Suter, D. M., and P. Forscher. 2001. Transmission of growth cone traction force through apCAM-cytoskeletal linkages is regulated by Src family tyrosine kinase activity. *J. Cell Biol.* 155:427–438.

41. Suter, D. M., A. W. Schaefer, and P. Forscher. 2004. Microtubule dynamics are necessary for Src family kinase-dependent growth cone steering. *Curr. Biol.* 14:1194–1199.

42. Lee, A. C., and D. M. Suter. 2008. Quantitative analysis of microtubule dynamics during adhesion-mediated growth cone guidance. *Dev. Neurobiol.* 68:1363–1377.

43. Schaefer, A. W., V. T. Schoonderwoert, …, P. Forscher. 2008. Coordination of actin filament and microtubule dynamics during neurite outgrowth. *Dev. Cell.* 15:146–162.

44. Lee, A. C., B. Decourt, and D. Suter. 2008. Neuronal cell cultures from *Aplysia* for high-resolution imaging of growth cones. *J. Vis. Exp.* http://dx.doi.org/10.3791/662.

45. Karhu, E., M. Gooyers, and J. L. Hutter. 2009. Quantitative friction-force measurements by longitudinal atomic force microscope imaging. *Langmuir.* 25:6203–6213.

46. Timoshenko, S., and J. M. Gere. 1997. Mechanics of Materials. PWS-Kent Pub. Co., Boston.

47. Butt, H. J., and M. Jaschke. 1995. Calculation of thermal noise in atomic force microscopy. *Nanotechnology.* 6:1.

48. Lozano, J. R., D. Kiracofe, …, A. Raman. 2010. Calibration of higher eigenmode spring constants of atomic force microscope cantilevers. *Nanotechnology.* 21:465502.

49. Oppenheim, A. V., and R. W. Schafe. 1975. Digital Signal Processing. Prentice-Hall, Englewood Cliffs, NJ.

50. Schneider, C. A., W. S. Rasband, and K. W. Eliceiri. 2012. NIH image to ImageJ: 25 years of image analysis. *Nat. Methods.* 9:671–675.

51. Decourt, B., V. Munnamalai, …, D. M. Suter. 2009. Cortactin colocalizes with filopodial actin and accumulates at IgCAM adhesion sites in *Aplysia* growth cones. *J. Neurosci. Res.* 87:1057–1068.

52. Thompson, C., C. H. Lin, and P. Forscher. 1996. An *Aplysia* cell adhesion molecule associated with site-directed actin filament assembly in neuronal growth cones. *J. Cell Sci.* 109:2843–2854.

53. Martines, E., J. Zhong, …, G. U. Lee. 2012. Single-molecule force spectroscopy of the *Aplysia* cell adhesion molecule reveals two homophilic bonds. *Biophys. J.* 103:649–657.

54. Choquet, D., D. P. Felsenfeld, and M. P. Sheetz. 1997. Extracellular matrix rigidity causes strengthening of integrin-cytoskeleton linkages. *Cell.* 88:39–48.

55. Saez, A., A. Buguin, …, B. Ladoux. 2005. Is the mechanical activity of epithelial cells controlled by deformations or forces? *Biophys. J.* 89:L52–L54.

56. Ghibaudo, M., A. Saez, …, B. Ladoux. 2008. Traction forces and rigidity sensing regulate cell functions. *Soft Matter.* 4:1836–1843.

57. Trichet, L., J. Le Digabel, …, B. Ladoux. 2012. Evidence of a large-scale mechanosensing mechanism for cellular adaptation to substrate stiffness. *Proc. Natl. Acad. Sci. USA.* 109:6933–6938.

58. Yip, A. K., K. Iwasaki, …, Y. Sawada. 2013. Cellular response to substrate rigidity is governed by either stress or strain. *Biophys. J.* 104:19–29.

59. Flanagan, L. A., Y.-E. Ju, …, P. A. Janmey. 2002. Neurite branching on deformable substrates. *Neuroreport.* 13:2411–2415.

60. Jiang, F. X., B. Yurke, …, N. A. Langrana. 2008. Neurite outgrowth on a DNA crosslinked hydrogel with tunable stiffnesses. *Ann. Biomed. Eng.* 36:1565–1579.

61. Plotnikov, S. V., A. M. Pasapera, …, C. M. Waterman. 2012. Force fluctuations within focal adhesions mediate ECM-rigidity sensing to guide directed cell migration. *Cell.* 151:1513–1527.

62. Vogel, V., and M. Sheetz. 2006. Local force and geometry sensing regulate cell functions. *Nat. Rev. Mol. Cell Biol.* 7:265–275.

63. He, S., Y. Su, …, H. Gao. 2014. Some basic questions on mechanosensing in cell-substrate interaction. *J. Mech. Phys. Solids.* 70:116–135.